Icarus 281 (2017) 281–285

Contents lists available at ScienceDirect

Icarus

journal homepage: www.elsevier.com/locate/icarus

Temperatures and CH_4 mixing ratios near the homopause of the 8 μm north polar hot spot of Jupiter

Sang Joon Kim[a,*], Thomas R. Geballe[b], Thomas K. Greathouse[c,1], Yuk L. Yung[d], Steve Miller[e], G.S. Orton[f], Y.C. Minh[g]

[a] School of Space Research, Kyung Hee University, Yongin, 446-701, Korea
[b] Gemini Observatory, 670 N. A'ohoku Place, Hilo, HI 96720, USA
[c] Southwest Research Institute, 6220 Culebra Road, San Antonio, TX 78238, USA
[d] Division of Geological and Planetary Sciences, Caltech, Pasadena, CA 91125, USA
[e] Department of Physics and Astronomy, University College London, London WC1E 6BT, U.K.
[f] Jet Propulsion Laboratory, California Institute of Technology, 4800 Oak Grove Drive, Pasadena, CA 91109, USA
[g] Korea Astronomy and Space Science Institute, Yuseong-gu, Daejeon 305-348, Korea

ARTICLE INFO

Article history:
Available online 13 September 2016

Keywords:
Jupiter
Atmosphere
Aurora
Infrared
Spectroscopy

ABSTRACT

We have derived homopause temperatures of 180–250 K for the 8-μm north-polar hot spot (8NPHS) of Jupiter by fitting CH_4 emission models to 3 and 8 μm spectra of the 8NPHS obtained 24 days apart in 2013. From the fits, we find that CH_4 mixing ratios at the 8NPHS are consistent with those reported by Kim et al. (2014) in equatorial regions. We propose possible mechanisms to account for the temperature of the 8NPHS homopause, which is relatively cool compared with the temperatures of other auroral regions, including locally-fixed and transient but energetic auroral particle precipitation.

1. Introduction

The upper atmosphere of Jupiter has been studied since the days of the Voyager spacecraft (e.g., Atreya, et al. 1981; Drossart et al. 1989; Miller et al. 1997), but the relationship between the region above the homopause where chemical species settle out according to their atomic or molecular weights and the region below where the atmosphere is well mixed has not been quantified. This is especially true in the polar zones near the so-called "hot spots" where IR emission from vibration-rotation bands of hydrocarbons is enhanced. The stratosphere (0.1–10 mbar pressure range) of the 8 μm CH_4 north-polar hot spot (8NPHS) is known to be ~20 K warmer than the surrounding polar region (e.g., Kim et al. 1985), but there is significant uncertainty in temperatures and CH_4 mixing ratios near the homopause (0.1–10 μbar pressure range) (Drossart et al. 1993).

The location of the 8NPHS has been observed to be stationary at 180° (SysIII) longitude since the early 1980s (e.g., Caldwell et al. 1983; Sada et al. 2003), whereas the south-polar hot spot has been observed to wander between 268°W and 96°E (SysIII) longitude (Caldwell et al. 1988). Recently, from an analysis of spectro-images of the north polar region (Figs. 1 and 2a) observed by the Gemini Near-Infrared Spectrograph (GNIRS) at Gemini North on January 13, 2013(UT), Kim et al. (2015) reported that the 3 μm CH_4 north-polar hot spot (3NPHS) is located at ~197° longitude (SysIII), significantly displaced from the center of the 8NPHS. They also tentatively concluded that temperature at the location of the 8NPHS homopause is less than 350 K (measured via the 3 μm emission found there), significantly lower than the temperature of 500 K measured at the displaced location of the maximum 3NPHS emission.

For the derivations of temperatures, Kim et al. (2015) considered only the *Q*-branch lines of the fundamental (ν_3) and hot ($\nu_3+\nu_4-\nu_4$ and $\nu_2+\nu_3-\nu_2$) bands of CH_4 at 3.31–3.34 μm, disregarding the seven much stronger *P*-branch lines of the ν_3 at 3.33–3.41 μm, which can be compromised by absorption due to their telluric counterparts (Fig. 1). If their strengths are measurable, however, these *P*-branch lines can also yield meaningful information on the temperature.

In this paper, we utilize the seven observed *P*-branch lines, P(2)-P(8), along with a high-resolution spectrum of a small portion of the ν_4 band of CH_4 near 8.0 μm (Fig. 2b) obtained with TEXES, the Texas Echelon Cross Echelle Spectrograph (Lacy et al. 2002), at the NASA Infrared Telescope Facility (IRTF) on Feb. 6, 2013(UT) only 24 days after the GNIRS/Gemini North observations, in order to

* Corresponding author.
E-mail address: sjkim1@khu.ac.kr (S.J. Kim).

[1] Visiting Astronomer at the Infrared Telescope Facility, which is operated by the University of Hawaii under contract NNH14CK55B with the National Aeronautics and Space Administration.

http://dx.doi.org/10.1016/j.icarus.2016.09.017
0019-1035/

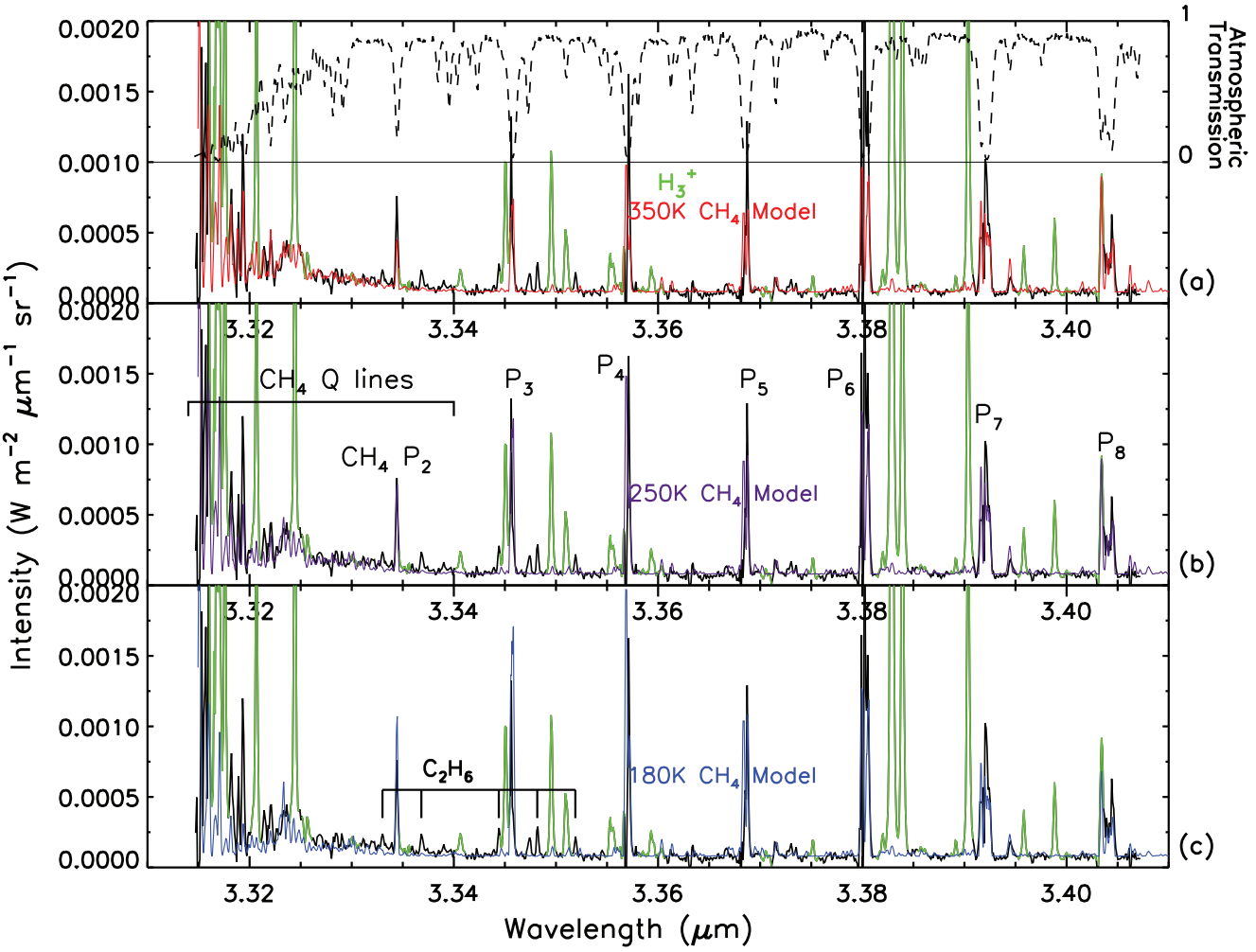

Fig. 1. a) GNIRS/Gemini North spectrum (black) of the 8NPHS compared with a model spectrum (red) with a temperature of 350 K of CH_4 bands. The wavelength ranges where H_3^+ lines dominate are shown in green. The atmospheric transmission (dashed line) is the standard star spectrum. The uncertainty of the GNIRS 8NPHS spectrum varies significantly depending on the telluric absorption, and the 1-σ noise level is ~0.0001 Wm^{-2}μm^{-1}sr^{-1} at the continuum where the atmospheric transmission is at least 70%. b) A comparison between the GNIRS 8NPHS spectrum (black) and a 250 K model (violet) of the CH_4 bands. *P*-branch lines of the CH_4 bands are indicated, as well as the wavelength range of the *Q*-branches. Each of the *Q*-branch emission features is a blend of many lines. c) A comparison between the GNIRS 8NPHS spectrum (black) and a 180 K model (blue) of the CH_4 bands. Identified C_2H_6 lines are marked. (For interpretation of the references to colour in this figure legend, the reader is referred to the web version of this article.)

narrow down the huge uncertainties in the temperature-pressure (T-P) and the CH_4 mixing-ratio profiles near the homopause of the 8NPHS (e.g., Drossart et al. 1993). We assume no significant thermal variation in the line emission at the 8NPHS between the times of the Gemini North and IRTF observations, based on the thermal stability in the stratosphere (Caldwell et al. 1979; Conrath et al. 1990; Zhang et al. 2013), where radiative response times are significantly longer than the 24 days between the two sets of observations.

2. Observations

The 3.31–3.41 μm spectrum of the 8NPHS was observed in photometric conditions at Gemini North on Jan. 13, 2014 (UT) using GNIRS' 111 l/mm grating and a 0.1″ × 49″ slit, which provided a spectral resolving power, R = λ/Δλ, of ≈18,000 (velocity resolution 16 km/s) . The relative velocity of Earth and Jupiter was ~20.6 km/sec, which allowed the partial separation of the lines of the fundamental ν_3 band of CH_4 from their telluric counterparts. These observations and the data reduction have been described by Kim et al. (2015); therefore, we only present here the observational parameters which are relevant to our analysis. The slit was oriented perpendicular to the central meridian and stepped in latitude from just off the north pole toward lower latitudes using 0.8″ steps with an exposure time of 4 min for each latitude. The 3 μm seeing was 0.5–0.6″. An image of the emission in the strong ν_3 band lines made from these data is shown in Fig. 2a, with the 8NPHS region represented as a dashed oval. The 3 μm flux-calibrated spectrum summed over the region of the 8NPHS is presented in Fig. 1. The uncertainty in the flux levels of individual data points in this spectrum varies significantly with wavelength, due to the presence of numerous strong telluric absorption lines. The 1-σ noise level is ~0.0001 Wm^{-2}μm^{-1}sr^{-1} on the continuum at wavelengths where the atmospheric transmission is at least 70%.

The spectrum of the 8NPHS between 7.990 and 8.035 μm was obtained with TEXES (Lacy et al. 2002) mounted on the IRTF on Feb. 6, 2013(UT), when the relative velocity of Earth and Jupiter was ~27 km/sec. TEXES was used in its medium-resolution mode with a 1.4″ × 45″ slit, resulting in a spectral resolving power, R, of ≈19,000, nearly identical to that of GNIRS. Jupiter's angular diameter was 42.2″. The slit was aligned along celestial N/S with the slit center located at the center of Jupiter. The slit was then offset 28″ West (off of Jupiter's limb), and then stepped by 0.7″ to

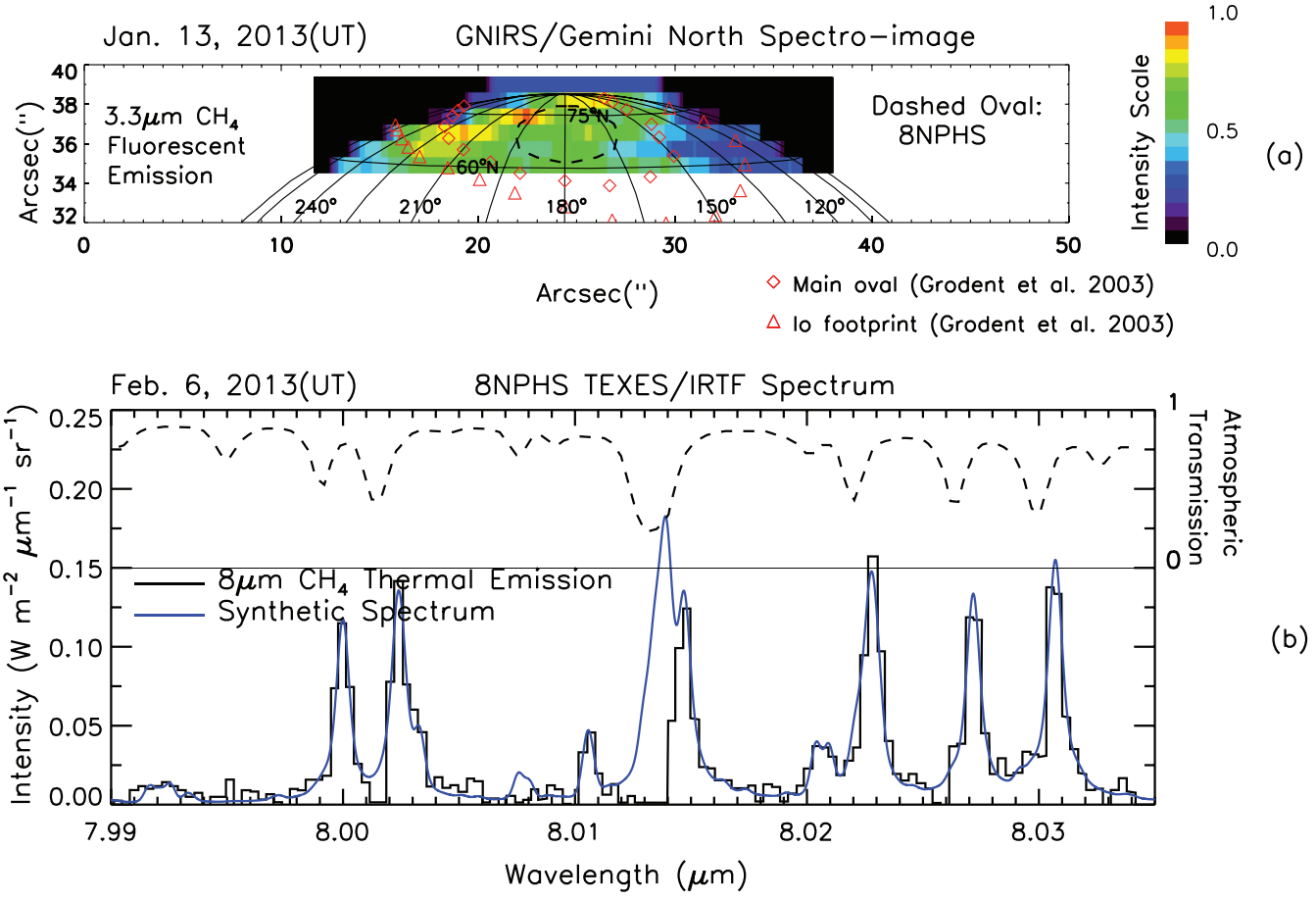

Fig. 2. a) A spectro-image of the 3.3 μm CH_4 band emission adopted from the second figure panel in Fig. 1 of Kim et al. (2015). The region of the 8NPHS is marked by dashed oval. b) A TEXES/IRTF spectrum (black) of the 8NPHS compared with a model spectrum (blue) using the temperatures and CH_4 mixing ratios presented in Fig. 3, which are derived from the analyses of the 3 μm GNIRS 8NPHS spectrum (Fig. 1). The atmospheric transmission (dashed) is made from an atmospheric transmission tool (http://atran.sofia.usra.edu/cgi-bin/atran/atran.cgi). The S/N ratios vary significantly depending on the atmospheric transmission, and the S/N is worst near 8.014 μm where the transmission is also worst; and the 1-σ noise level is ~0.02 $Wm^{-2}\mu m^{-1}sr^{-1}$ where the transmission is at least 70%. (For interpretation of the references to colour in this figure legend, the reader is referred to the web version of this article.)

the east 80 times in order to scan across Jupiter and include sky frames on either side. The exposure time per step was 2 s. The extracted spectrum from the 8NPHS region is shown in Fig. 2b along with a model spectrum for a comparison. The S/N ratios vary significantly depending on the atmospheric transmission as perceived in the detailed fits between the model and observation; and the 1-σ noise level is ~0.02 $Wm^{-2}\mu m^{-1}sr^{-1}$ at wavelengths where the atmospheric transmission is at least 70%.

3. Derivations of T-P and CH_4 Mixing-ratio profiles at the 8NPHS

In this section, we derive 8NPHS T-P and CH_4 mixing-ratio profiles from the 3 μm and 8 μm spectra, and compare them with previous results from Voyager IRIS spectra (Drossart et al. 1993). Because the peak contribution to the 3 μm CH_4 ν_3 band emission occurs at higher altitude (~1 μbar) than does the peak contribution to the 8 μm CH_4 ν_4 band emission (~1 mbar), it is possible to constrain the T-P and CH_4 mixing-ratio profiles over a wide vertical range (i.e., 1 μbar ~1 mbar). Radiative transfer programs and HITRAN2012 CH_4 line parameters (Rothman et al. 2009) used for this analysis have been described in detail by Kim et al. (2014), and the sensitivity tests of Kim et al. (2014) are adopted here for the derivations of uncertainties in the mixing-ratio and T-P profiles.

We consider not only model fits to the *rotational structures* of the 3 μm CH_4 lines for the derivation of rotational temperatures, which are in fact the local temperatures as discussed by Kim et al. (2014), but also fits to the *absolute intensities* of the CH_4 lines for the derivation of CH_4 mixing ratios. Regarding the absolute intensity fit, we note that the 8NPHS region is relatively dark within the main oval as shown in the 3 μm H_3^+ and CH_4 images presented in Fig. 1 of Kim et al. (2015). That suggests relatively low auroral activity between *nano*bar and μbar pressure range at the 8NPHS. Furthermore, after spectral convolution with the ISO (Infrared Space Observatory) resolution, the 3 μm CH_4 intensities of the 8NPHS in Fig. 1 are found to be very similar to those of the equatorial spectra (Kim et al. 2014) measured by ISO, indicating low auroral activity near the homopause (~1 μbar) at the 8NPHS. At present the detailed auroral activity within the auroral oval is not known to sufficient accuracy to derive meaningful CH_4 mixing ratios there. The intensity similarity between the equatorial and 8NPHS spectra, however, provides an opportunity to derive rough CH_4 mixing ratios near 1 μbar, assuming that the 3 μm CH_4 emission there is mostly caused by fluorescence of solar radiation, for which details are quantitatively known. For the equatorial region, Kim et al. (2014) derived a range of CH_4 mixing ratios (the hatched area in Fig. 3a) from the 3 μm ISO spectrum. We expect a similar range of mixing ratios for the 8NPHS region because the two spectra are very similar after accounting for the difference in pathlengths, due to the different sightlines through the upper atmospheres.

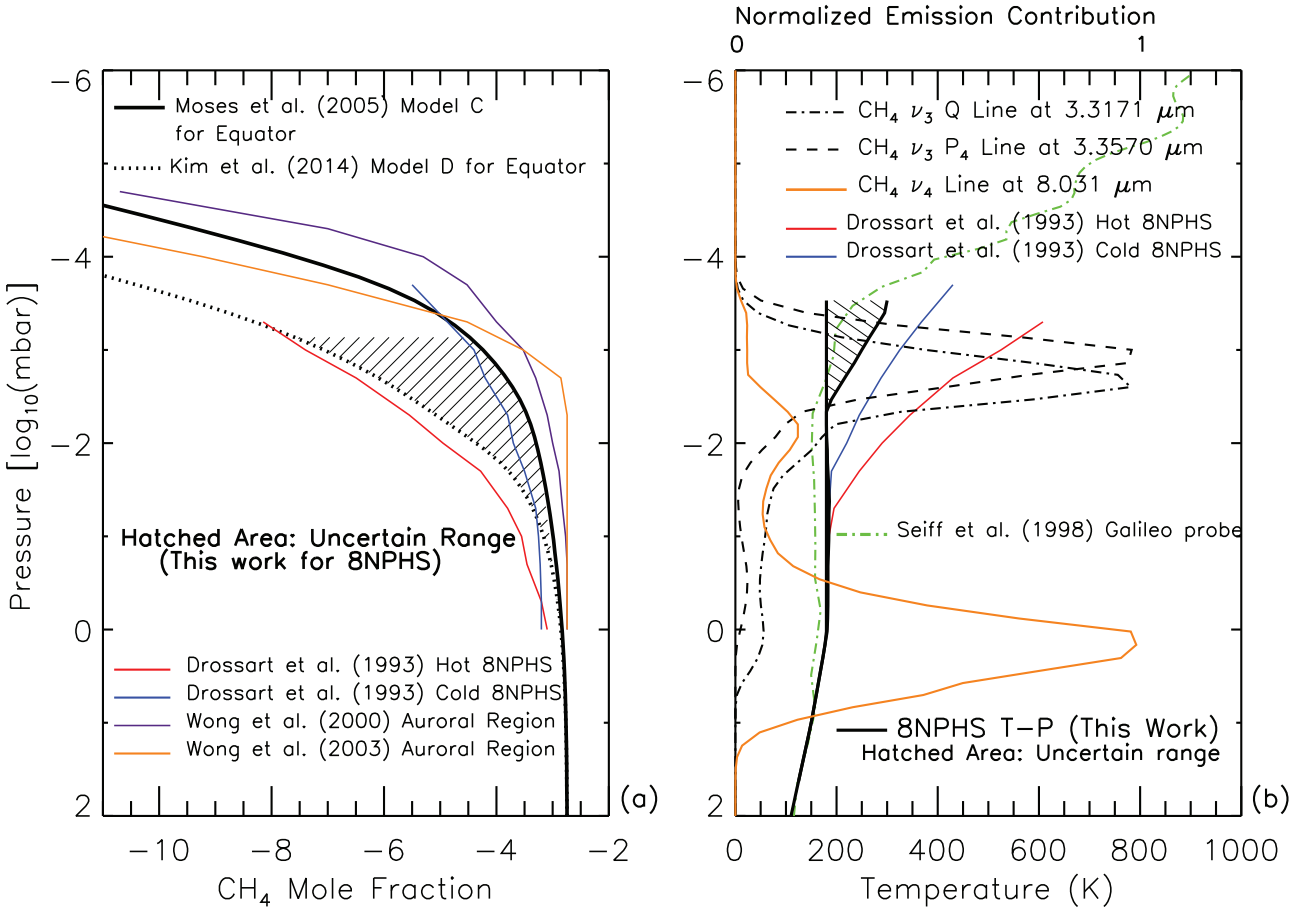

Fig. 3. a) Derived CH_4 mole fractions vs. pressure. The hatched range is the uncertainty in the derived mole fractions. Previously reported observational and theoretical results are also presented for comparison. b) Derived T-P profiles of this work compared with the cold and hot T-P profiles derived from Voyager IRIS data (Drossart et al. 1993) and an equatorial T-P profile from the *in-situ* Galileo probe (Seiff et al. 1998). Emission contribution curves for the 3 and 8 μm CH_4 lines are also shown. The hatched area is an uncertainty in the temperatures derived from this work.

For the 8NPHS homopause temperature, we first check the hot and cold T-P models presented in Fig. 9 of Drossart et al. (1993), which have ~520 K and ~320 K near 1 μbar, respectively. Their cooler model is consistent with the result ($T < 350$ K) of Kim et al. (2015), but we note that the absolute intensity of the TEXES 8NPHS spectrum after spectral convolution with the Voyager IRIS resolution is found to be approximately 1.5 times less than that of the IRIS spectra measured in 1979, suggesting possible long-term variation.

To fine-tune the fit to the 3 μm *P*- and *Q*- branch lines of CH_4 (Fig. 1b), we take advantage of the fact that the *Q*-branch observations of the combination bands near 3.32μm cover all rotational levels while the ν_3 *P*-branch coverage only includes lines with $J < 7$. Thus the intensity ratio of the observed *Q*-branch and partially observed *P*-branch is sensitive to the rotational temperature. In Fig. 1a,b,and c, fits of CH_4 models with 350, 250, and 180 K to the 3 μm 8NPHS spectrum are presented. The continuum level, caused mainly by polar haze, is 8×10^{-5} W $m^{-2}\mu m^{-1} sr^{-1}$, and is relatively flat in this wavelength range. We forced our model to fit the 8NPHS spectrum at the *Q*-branches and then watch the intensities of the model *P* lines vary with temperature. For the 350 K case, except for the *P*(8) line, all of the *P*-branch line intensities are less than the observed intensities indicating that the rotational temperature is less than 350 K. For the 250 and 180 K cases, the number of lines weaker or stronger than the observed lines seems roughly balanced indicating that the derived homopause temperature at the 8NPHS is between 180 K and 250 K.

The derived T-P and CH_4 mixing-ratio profiles from the GNIRS spectra along with uncertainties marked by hatched lines are presented in Fig. 3a and b. Hopefully, the upcoming JUNO observations of the polar regions of Jupiter during the encounter with the Jovian system will provide more complete and cleaner coverage of the CH_4 ν_3 *P*- and *R*-branches.

Using the 8 μm TEXES data, we attempt to confirm the derived T-P and CH_4 mixing-ratio curves, because a secondary contribution peak to the 8 μm CH_4 emission occurs around 1 μbar (Fig. 3b). In Fig. 2b we present a satisfactory fit to the TEXES spectrum by a synthetic spectrum made with the Model C mixing ratio in Fig. 3a, and with a T-P curve in the hatched area in Fig. 3b. We find that all of the model spectra made using the CH_4 mixing-ratio and T-P curves in the hatched areas in Fig. 3a and 3b produce very similar 8 μm model spectra, each matching the observed spectrum to within its uncertainties. We also note that the analysis of the 3 μm ISO spectrum by Kim et al. (2014) produced a lower limit to the CH_4 mixing ratio at μbar levels (i.e., Model D in their Fig. 4 and our Fig. 3a). The lower limit is due to the very large uncertainty in the vibrational relaxation rate of the CH_4 ν_3 band. Model D is still valid for the lower-limit mixing ratios at the μbar levels of the 8NPHS, since the relaxation rate is not accurately known. The hatched area in the T-P curves in Fig. 3b is obtained by considering the uncertainties in correcting for the telluric absorption due to the partial separations of the Jovian CH_4 ν_3 lines from their telluric counterparts despite the large Doppler shift as mentioned in Section 2.

To summarize, considering all the effects of temperature and mixing ratio on the model fits as presented above, we find that a simultaneous fit to the 3 μm-GNIRS (Fig. 1) and 8 μm-TEXES spectra (Fig. 2) can be obtained with the synthetic spectra made from the mixing-ratio and the T-P profiles with uncertainties marked by hatched lines shown in Fig. 3a and b. At 1 μbar the derived temperature range is between 180 K and 250 K.

4. Discussions and conclusions

Ionization of hydrocarbon molecules by solar radiation occurs in the high-altitude Jovian stratosphere above the homopause (Kim, Y., and Fox, 1994). In the auroral regions, the ionization is increased by particle bombardment, and thus the temperatures near the homopause must be higher than in non-auroral regions. The apparently cool homopause temperature measured at the 8NPHS in this work indicates that the influence of auroral activities on the homopause region of the 8NPHS is very low, and then the heat source in the stratosphere of the 8NPHS may be due to other mechanisms: e.g., a dynamical mechanism, such as heat dissipation of fixed planetary waves in the stratosphere (French and Gierasch, 1974), or absorption of sunlight by high-altitude polar haze (Axel, 1972). A transient polar haze, whose size and location are about the same as those of the 8NPHS region, was detected by Cassini/ISS (Li, et al., 2006), but it is not known at present whether (i) the haze causes the 8NPHS heating, (ii) is a result of the heating, or (iii) is irrelevant to the heating. Here, we note the possibility of a transient but locally-fixed auroral beam, which did not occur during our observations, but that would be energetic enough to create the 8NPHS at mbar pressure levels (Kim, 1988). There, the heat capacity is higher than at the homopause altitude so that the high temperatures can be maintained at least for several months (Caldwell, et al. 1979; Conrath, et al. 1990; Zhang et al. 2013) until the next auroral beam occurs. This high-energy particle beam may also initiate a chemical process to form the transient polar haze detected by the Cassini/ISS. Additional 3 μm observations are certainly needed to confirm or rule out this possibility.

Theoretical CH_4 mixing ratios resulted from chemical models for the Jovian auroral regions reported by Wong et al. (2000; 2003) are generally greater than our results between pressures of 0.1 and 10 μbar (Fig. 3a). However, since their results are for the active auroral regions, and the auroral activities at 8NPHS were very low at the time of our observations, a direct comparison may not be very meaningful. One of us (YLY) is now preparing a full paper presenting an updated version of hydrocarbon mixing ratios and chemistry for the auroral regions of Jupiter.

Acknowledgments

SJK acknowledges support from the Space Core Technology program through NRF funded by the Ministry of Education, Science and Technology, and from KASI under the R&D program supervised by the Ministry of Science, ICT and Future Planning. Support for GSO was provided, in part, by an award from NASA to the Jet Propulsion Laboratory, California Institute of Technology. The research is based in part on observations obtained at the Gemini Observatory, which is operated by the Association of Universities for Research in Astronomy, Inc., under a cooperative agreement with the NSF on behalf of the Gemini partnership: the National Science Foundation (United States), the National Research Council (Canada), CONICYT (Chile), Ministerio de Ciencia, Tecnología e Innovación Productiva (Argentina), and Ministério da Ciência, Tecnologia e Inovação (Brazil).

References

Atreya, S.K., Donahue, T.M., Festou, M.C., 1981. Jupiter: structure and composition of the upper atmosphere. Astrophys. J. 247, L43–L47.
Caldwell, J., et al., 1979. Temporal characteristics of the Jovian atmosphere. Astrophys. J. 234, L155–L158.
Caldwell, J., Tokunaga, A.T., Orton, G.S., 1983. Further observations of 8-μm polar brightenings of Jupiter. Icarus 53, 133–140.
Caldwell, J., et al., 1988. Infrared polar brightenings on Jupiter IV. Spatial properties of methane emission. Icarus 74, 331–339.
Conrath, B.J., Gierasch, P.J., Leroy, S.S., 1990. Temperature and circulation in the stratosphere of the outer planets. Icarus 83, 255–281.
Drossart, P., et al., 1989. Detection of H_3^+ on Jupiter. Nature 340, 539–541.
Drossart, P., et al., 1993. Thermal profiles in the auroral regions of Jupiter. J. Geophys. Res. 98, 18803–18811.
French, R.G., Gierasch, P.J., 1974. Waves in the Jovian upper atmosphere. J. Atm. Sci. 31, 1707–1712.
Kim, S.J., 1988. Infrared processes in the Jovian auroral zone. Icarus 75, 399–408.
Kim, S.J., et al., 1985. Infrared polar brightening on Jupiter. III. Spectrometry from the Voyager 1 IRIS experiment. Icarus 64, 233–248.
Kim, S.J., et al., 2014. CH_4 mixing ratios at microbar pressure levels of Jupiter as constrained by 3-micron ISO data. Icarus 237, 42–51. http://dx.doi.org/10.1016/j.icarus.2014.04.023.
Kim, S.J., et al., 2015. Hot CH_4 in the polar regions of Jupiter. Icarus 257, 217–220. http://dx.doi.org/10.1016/j.icarus.2015.05.008.
Kim, Y.H., Fox, J.L., 1994. The chemistry of hydrocarbon ions in the Jovian ionosphere. Icarus 112, 310–325. doi:10.1006/icar.1994.1186.
Lacy, J.H., Richter, M.J., Greathouse, T.K., Jaffe, D.T., Zhu, Q., 2002. TEXES: a sensitive high-resolution grating spectrograph for the mid-infrared. Publ. Astron. Soc. Pac. 114, 153–168.
Li, L., et al., 2006. Waves in Jupiter's atmosphere observed by the Cassini ISS and CIRS instruments. Icarus 185, 416–429. doi:10.1016/j.icarus.2006.08.005.
Miller, S., et al., 1997. Mid-to-low latitude H_3^+ emission from Jupiter. Icarus 130, 57–67.
Rothman, L.S., et al., 2009. The HITRAN 2008 molecular spectroscopic database. J. Quant. Spectrosc. Radiat. Trans. 110, 533–572. http://dx.doi.org/10.1016/j.jqsrt.2009.02.013.
Sada, P.V., et al., 2003. Transient IR phenomena observed by Cassini/CIRS in Jupiter's auroral regions. Bull. Amer. Astron. Soc. 35, 402.
Seiff, A., et al., 1998. Thermal structure of Jupiter's atmosphere near the edge of a 5-μm hot spot in the north equatorial belt. J. Geophys. Res. 103, 22857–22889. http://dx.doi.org/10.1029/98JE01766.
Wong, A.-S., Lee, A.Y.T., Yung, Y.L., 2000. Jupiter: aerosol chemistry in the polar atmosphere. Astrophys. J. 534, L215–L217.
Wong, A.-S., Yung, Y.L., Friedson, A.J., 2003. Benzene and haze formation in the polar atmosphere of Jupiter. Geophys. Res. Lett. 30. http://dx.doi.org/10.1029/2002GL016661.
Zhang, X., Nixon, C.A., Shia, R.L., West, R.A., Irwin, P.G., Yelle, R.V., Allen, M.A., Yung, Y.L., 2013. Radiative forcing of the stratosphere of Jupiter, Part I: atmospheric cooling rates from Voyager to Cassini. Planet Space Sci 88, 3–25. http://dx.doi.org/10.1016/j.pss.2013.07.0035.